A NEW NON-ORTHODOX MULTIPOINT FLUX APPROXIMATION METHOD (MPFA-HD) FOR THE SIMULATION OF ONE-PHASE PROBLEMS IN ANISOTROPIC AND HETEROGENEOUS POROUS MEDIA

[1]**Contreras Fernando RL**

ferlicapac@gmail.com

[2]**Lyra Paulo RM**

[3]**Carvalho Darlan KE**

prmlyra@padmec.org

dkarlo@oul.com.br

[1]Centro Acadêmico do Agreste, UFPE, Rodovia BR 104 KM 59, 55002-970, Caruaru, PE-Brazil. [2,3]Departamento de Engenharia Mecânica, UFPE, Av. Acadêmico Hélio Ramos s/n, 50670-901, Recife, PE-Brazil.

Abstract. *In the present paper, we present a new linear cell-centered finite volume method with a Multipoint Flux Approximation (MPFA-HD) that uses a quasi-local stencil to approximate the steady-state one-phase flow problem in porous medium using arbitrarily polygonal meshes that reproduces piecewise linear solutions exactly. The derivation of our linear MPFA-HD scheme is based on recently developed Non-Linear Finite Volume (NLFV) methods that are aimed to produce monotone solutions even for highly distorted meshes and strongly anisotropic media. In our linear scheme, we first construct the one-sided fluxes on each control surface independently and then a unique flux expression is obtained by a convex combination of the one-sided fluxes. In order to improve the performance of our linear scheme for highly anisotropic diffusion tensors, and differently from other classical MPFA methods, in our scheme, fluxes on each cell face are explicitly expressed by two cell centered unknowns belonging to two adjacent control volumes and points defined on vertices that do not necessarily belong to the same face shared by the adjacent cells, leading eventually to a non-local stencil. The unknown values at the required vertices are obtained by means of a linear preserving interpolation procedure, considering the surrounding control volumes to such vertices. To show the potential of our MPFA-HD finite volume formulation, we solve some benchmark problems found in literature.*

Keywords: *One-Phase Flow, Anisotropic and Heterogeneous Porous Medium, MPFA-HD Finite Volume.*

1 INTRODUCTION

Diffusion processes based on conservations laws are present in several engineering applications, such as heat propagation or flows in porous media encountered in reservoir engineering. These physical phenomena are mathematically described by equations that have an elliptic operator with a diffusion coefficient, which is, in general, discontinuous and represented by a tensor that usually can present a high-anisotropy ratio (Queiroz et al., 2013, Droniou, 2014). Accurate modeling of diffusion processes in these applications requires reliable discretization methods.

In this paper, we are interested in constructing a cell-centered finite volume scheme which satisfies the following properties:

- it is locally conservative;
- it satisfies the Discrete Extremum Principle (DMP);
- it must be reliable on unstructured anisotropic meshes that may be highly distorted;
- it allows heterogeneous full tensors;
- it has a second-order accuracy for smooth solutions.
- it reproduces piecewise linear solutions exactly.

These properties were suggested initially by Lipnikov et al., (2007) and Yuan and Sheng (2008) to characterize an ideal numerical method developed to solve elliptic problems. The second property is the most difficult one for a discrete scheme to satisfy. The DMP or at least monotonicity is very important in different areas of application, for instance, in the context of oil reservoir simulation, unphysical oscillations in the discrete solution are undesirable in any application, but for multiphase flow, such oscillations may have serious consequences. If the computed pressure lies below the bubble-point curve of the mixture, while the actual pressure lies above it, artificial gas may be liberated, yielding a strongly diverging solution (Nordbotten et al., 2007). Therefore, an oscillation-free solution of the elliptic model equation is desired.

Classical discretization schemes for diffusion problem include linear: finite-differences (FD), finite-element (FE) or finite-volume (FV) methods. Whenever applying these schemes to diffusion problem with a strongly anisotropic full-tensor field they can fail to satisfy the maximum principle, resulting in spurious oscillations in the numerical solution. In an attempt to mitigate these problems, for challenging cases, a new generation of numerical linear and non-linear locally conservative formulations have been proposed in literature (Edwards e Zheng, 2008; Chen et al., 2008; Aavatsmark et al., 2008; Gao e Wu, 2011).

For diffusion problems with slightly anisotropic diffusion tensors and with non-distorted quadrilateral meshes, the classical MPFA-O scheme can adequately represent the pressure field. However, as it was shown by Nordbotten and Aavatsmark (2007) the MPFA-O scheme fails to satisfy the maximum principle for strong anisotropies or grid skewness. To improve the robustness of the classical MPFA-O scheme, Edwards and Zheng (2008) proposed a MPFA with Full Pressure Support (MPFA-FPS) that can reduce the numerical oscillations in general unstructured meshes for problems with highly anisotropic diffusion tensors or whenever using strongly distorted meshes.

In this paper, the mathematical model is discretized by a non-orthodox cell-centered Multi-Point Flux Approximation (MPFA) Method with a Half-Diamond stencil (MPFA-HD). This method was based on the classical non-linear method to solve diffusion problems in strongly heterogeneous and anisotropic media using general polygonal meshes in two dimensions (Le Potier, 2005; Lipnikov et al., 2007; Yuan and Sheng, 2008). In our method, as in other finite volume schemes the key point is the discretization of the flux across each cell control surface (edge in 2-D). We first construct the one-sided fluxes on each cell independently and then, integrate the two one-sided fluxes on both sides. Finally, the cell edge fluxes are expressed as a convex combination of the one side fluxes to obtain a unique flux expression. In contrast to classical MPFA method (Aavastmark *et al*., 1998; Edwards and Rogers, 1998; Gao and Wu, 2011; Contreras et al., 2016), in the MPFA-HD method, the flux on each face is explicitly expressed by one cell centered unknown defined on the cells sharing that face and two auxiliary unknowns defined at two edge endpoints that do not necessarily belong to the same edge shared by the adjacent cells. As the scheme is cell-centered, auxiliary unknowns are expressed as weighted linear combinations of the neighboring cell-centered unknowns in order to reduce the scheme to a completely cell-centered one. In the method proposed by Gao and Wu (2011), the weights are neither discontinuity or mesh topology dependent as in some of the other previous methods and can be used even for full tensor problems. The derivation of the scheme and of these weights satisfy the linearity preserving criterion, which requires that a discretization scheme should be exact on piecewise linear solutions (Carvalho et al., 2006; Gao and Wu, 2011).

2 MATHEMATICAL FORMULATION

The equation that defines the two-dimensional steady-state diffusion problem in heterogeneous and anisotropic media can be written as:

$$\nabla \vec{\mathcal{F}} = Q(\vec{x}) \text{ and } \vec{\mathcal{F}} = -\underset{\sim}{K}(\vec{x})\nabla u \text{ in } \vec{x} = (x, y) \in \Omega \subset \mathbb{R}^2 \tag{1}$$

where Ω is an open bounded subset $\mathbb{R}^2$ with $\partial\Omega$ being its boundary, u is the variable pressure, the flux $\vec{\mathcal{F}}$ the Darcy's Law for porous media. And Q represents a source (or sink) term. In Cartesian coordinates, the diffusion tensor is usually represented by:

$$\underset{\sim}{K}(\vec{x}) = \begin{pmatrix} k_{xx} & k_{xy} \\ k_{yx} & k_{yy} \end{pmatrix} \tag{2}$$

Which is a positive-definite symmetric matrix that can be discontinuous through the open domain Ω.

The problem described by equation (1) is only completely defined when we use appropriate boundary conditions. Typical boundary conditions are given by:

$$\begin{aligned} u &= g_D \quad && on \quad \Gamma_D \neq \phi, \\ \vec{\mathcal{F}} \cdot \vec{n} &= g_N \quad && on \quad \Gamma_N \end{aligned} \tag{3}$$

where $\partial\Omega = \Gamma_D \cup \Gamma_N$, Γ_D represent the Dirichlet and Γ_N Neumann boundaries. The scalar function g_D (prescribed pressure) is defined in Γ_D and g_N (prescribed fluxes) is defined in Γ_N. Furthermore, $\vec{n}$ is the unit outward normal vector.

3 NUMERICAL FORMULATION

In this section, we present the numerical formulation of a non-orthodox Multipoint Flux Approximation Method (MPFA-HD), using an interpolation strategy proposed in (Gao and Wu, 2011).

3.1 Formulation of the MPFA-HD method

The discretization of the continuous domain is performed by an open set polygonal $\Omega \subset R^2$ with its boundaries denoted by $\partial\Omega = \bar{\Omega} \setminus \Omega$ (the closure of Ω is denoted by $\bar{\Omega}$). An admissible discretization (Eymard et al., 2000) involves the composition of three supersets denoted by $\mathcal{D} = (\mathcal{M}, \mathcal{E}, \mathcal{O})$, where:

• $\mathcal{M} = \{\hat{L}\}$ is a finite family of control volumes such that: $\bigcup_{\hat{L} \in \mathcal{M}} \bar{\hat{L}} = \bar{\Omega}$, where each control volume $\hat{L}$ is a star-shaped polygonal with respect to $x_{\hat{L}}$ (barycenter), which means that any ray emanating from $x_{\hat{L}}$ intersects the boundary of $\hat{L}$ at any one point (Lina C., 2014). The volume (area in 2D) of $\hat{L} \in \mathcal{M}$ is denoted by $V_{\hat{L}}$ and the cardinal of $\mathcal{M}$ is given by *n*.

• $\mathcal{E} = \{IJ\}$ is a finite family of edges in $\bar{\Omega}$, usually called control surfaces. For each $\hat{L} \in \mathcal{M}$, there exist a subset $\mathcal{E}_{\hat{L}}$ of $\mathcal{E}$ such that: $\bigcup_{IJ \in \mathcal{E}_{\hat{L}}} \overline{IJ} = \partial\hat{L}$. Also, we assume that for all $IJ \in \mathcal{E}$, we have $IJ \subset \partial\Omega$ or $IJ \subseteq \hat{L} \cap \hat{R}$, for some $(\hat{L}, \hat{R}) \in \mathcal{M} \times \mathcal{M}$. The set of internal and external edges are denoted, respectively by $\mathcal{E}^{\text{int}} = \mathcal{E} \cap \Omega$ and $\mathcal{E}^{ext} = \mathcal{E} \cap \partial\Omega$. Finally, the length of the edge *IJ* is given by the Euclidean norm $\|\overrightarrow{IJ}\|$.

Proceedings of the XXXVIII Iberian Latin-American Congress on Computational Methods in Engineering
P.O. Faria, R.H. Lopez, L.F.F. Miguel, W.J.S. Gomes, M. Noronha (Editores), ABMEC, Florianópolis, SC, Brazil, November 5-8, 2017.

$\bullet' = \left\{ x_{\hat{L}} \right\}_{\hat{L}\in\mathcal{M}}$ is a finite family of points (barycenter's of the control volumes) of Ω, so that, for all $\hat{L} \in \mathcal{M}$, $x_{\hat{L}} \in \hat{L}$.

Now, we integrate Equation (1) over the whole domain, yielding:

$$\int_{\Omega} \nabla \vec{\mathcal{F}} \, \mathrm{ds} = \int_{\Omega} Q dV \tag{4}$$

By applying the divergence theorem to the left-hand side of equation (4), we have:

$$\int_{\partial\Omega} \nabla \vec{\mathcal{F}} \cdot \vec{n} \, \mathrm{ds} = \int_{\Omega} Q dV \tag{5}$$

Considering a control volume approach in which $\hat{L} \in \mathcal{M}$ is a polygonal mesh (Figure 1), we can write:

$$\sum_{\hat{L}\in\mathcal{M}} \int_{\partial\hat{L}} \vec{\mathcal{F}} \cdot \vec{n} \, \mathrm{ds} = \sum_{\hat{L}\in\mathcal{M}} \int_{\hat{L}} Q_{\hat{L}} dV \ \text{ for all } \hat{L} \in \mathcal{M} \tag{6}$$

Therefore, the left and right sides of equation (6) can be approximated, respectively, as:

$$\int_{\partial\hat{L}} \vec{\mathcal{F}} \cdot \vec{n} \, \mathrm{ds} \cong \sum_{IJ\in\mathcal{E}_{\hat{L}}} \vec{\mathcal{F}}_{IJ} \cdot \vec{N}_{IJ} \quad \text{and} \quad \bar{Q}_{\hat{L}} V_{\hat{L}} = \int_{\hat{L}} Q_{\hat{L}} dV \tag{7}$$

where $\vec{\mathcal{F}}_{IJ} = \dfrac{1}{\left\| \overrightarrow{IJ} \right\|} \displaystyle\int_{IJ} \vec{\mathcal{F}} \, \mathrm{ds}$ and $\bar{Q}_{\hat{L}} = \dfrac{1}{V_{\hat{L}}} \displaystyle\int_{\hat{L}} Q_{\hat{L}} dV$.

In Equation (7), the numerical flux flow or flux density $\vec{\mathcal{F}}_{IJ} \cdot \vec{N}_{IJ}$ can be approximated in many ways, each one leading to different, linear or non-linear finite volume schemes (Edwards et al., 1998; Aavatsmark., 2002, Le Potier, 2005; Lipnikov et al., 2007; Yuan and Sheng, 2008; Gao and Wu, 2011). For a general control surface IJ of the mesh, this term must satisfy the local conservation equation, given, by:

$$\vec{\mathcal{F}}_{IJ} \cdot \vec{N}_{IJ} + \vec{\mathcal{F}}_{IJ} \cdot \vec{N}_{JI} = 0 \tag{8}$$

From equations (1) and (6), the one sided flux through a control surface IJ with respect to control volume $\hat{L}$, is expressed as:

$$\int_{IJ} \vec{\mathcal{F}} \cdot \vec{n}_{IJ} \mathrm{ds} = -\int_{IJ} \underset{\sim}{K}_{\hat{L}} \nabla u \cdot \vec{n}_{IJ} \mathrm{ds} = -\int_{IJ} \nabla u \cdot \underset{\sim}{K}_{\hat{L}}^{\mathsf{T}} \vec{n}_{IJ} \mathrm{ds} \text{, for each } IJ \in \mathcal{E}_{\hat{L}} \tag{9}$$

In Equation (9) the transpose of diffusion tensor is represented by $\underset{\sim}{K}_{\hat{L}}^{\mathsf{T}}$. We approximate the term $\nabla u \cdot \underset{\sim}{K}_{\hat{L}}^{\mathsf{T}} \vec{n}_{IJ}$ using the Taylor series expansion (Yuan and Sheng, 2008) on the "Half-Diamond" region showed in figure 1.

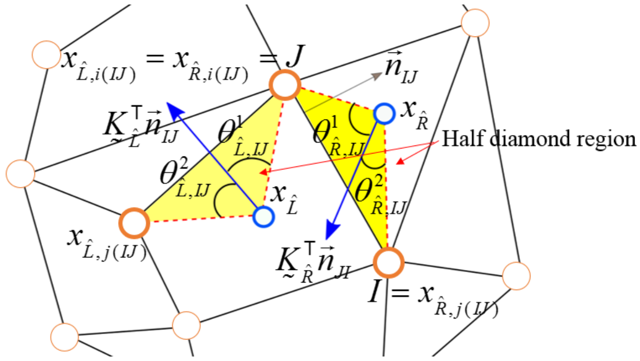

Figure 1. Some details of the MPFA-HD method: the physical-geometric parameters and the "Half-Diamond" region (yellow).

For instance, consider the triangle $\Delta x_{\hat{L}} x_{\hat{L},i(IJ)} x_{\hat{L},j(IJ)}$ of the figure 1. For this triangle, the co-normal $\underset{\sim}{K}_{\hat{L}}^{\mathsf{T}} \cdot \vec{n}_{IJ}$ always can be written as a convex combination of $\overrightarrow{x_{\hat{L}} x_{\hat{L},i(IJ)}}$ and $\overrightarrow{x_{\hat{L}} x_{\hat{L},j(IJ)}}$ since the control volume $\hat{L}$ is star-shaped, therefore, we can write:

$$\underset{\sim}{K}_{\hat{L}}^{\mathsf{T}} \vec{n}_{IJ} = \alpha_{\hat{L},i(IJ)} \overrightarrow{x_{\hat{L}} x_{\hat{L},i(IJ)}} + \alpha_{\hat{L},j(IJ)} \overrightarrow{x_{\hat{L}} x_{\hat{L},j(IJ)}} \tag{10}$$

where,

$$\alpha_{\hat{L},i(IJ)} \geq 0,\ \alpha_{\hat{L},j(IJ)} \geq 0 \text{ and } \alpha_{\hat{L},i(IJ)} + \alpha_{\hat{L},j(IJ)} \geq 0 \tag{11}$$

Equation (10) (with Equation (11)) is the so-called, convex decomposition of the co-normal (Shang and Yuan, 2016), this decomposition is necessary in constructing positive-preserving schemes, such as those in (Lepotier, 2005; Lipnikov et al., 2007; Yuan and Sheng, 2008). The physical-geometric parameters in Equation (11) are calculated following a geometric procedure. In fact, we can write:

$$\left|\alpha_{\hat{L},j(IJ)}\right| = \frac{\left\| \underset{\sim}{K}^{\mathsf{T}} \vec{n}_{IJ} \wedge \overrightarrow{x_{\hat{L}} x_{\hat{L},i(IJ)}} \right\|}{\left\| \overrightarrow{x_{\hat{L}} x_{\hat{L},j(IJ)}} \wedge \overrightarrow{x_{\hat{L}} x_{\hat{L},i(IJ)}} \right\|} \quad \text{and} \quad \sin\left(\theta^1_{\hat{L},IJ} + \theta^2_{\hat{L},IJ}\right) = \frac{\left\| \overrightarrow{x_{\hat{L}} x_{\hat{L},j(IJ)}} \wedge \overrightarrow{x_{\hat{L}} x_{\hat{L},i(IJ)}} \right\|}{\left\| \overrightarrow{x_{\hat{L}} x_{\hat{L},i(IJ)}} \right\| \left\| \overrightarrow{x_{\hat{L}} x_{\hat{L},j(IJ)}} \right\|} \tag{12}$$

where the angles $\theta^1_{\hat{L},IJ}$ and $\theta^2_{\hat{L},IJ}$ are represented in figure 1. From Equation (12), we have:

Proceedings of the XXXVIII Iberian Latin-American Congress on Computational Methods in Engineering
P.O. Faria, R.H. Lopez, L.F.F. Miguel, W.J.S. Gomes, M. Noronha (Editores), ABMEC, Florianópolis, SC, Brazil, November 5-8, 2017.

$$\left\|\overrightarrow{x_{\hat{L}}x_{\hat{L},j(IJ)}} \wedge \overrightarrow{x_{\hat{L}}x_{\hat{L},i(IJ)}}\right\| = \frac{\left\|\underset{\sim}{K}^{\mathsf{T}}\vec{n}_{IJ} \wedge \overrightarrow{x_{\hat{L}}x_{\hat{L},i(IJ)}}\right\|}{\left|\alpha_{\hat{L},j(IJ)}\right|} = \left\|\overrightarrow{x_{\hat{L}}x_{\hat{L},i(IJ)}}\right\|\left\|\overrightarrow{x_{\hat{L}}x_{\hat{L},j(IJ)}}\right\|\sin\left(\theta^1_{\hat{L},IJ} + \theta^2_{\hat{L},IJ}\right) \tag{13}$$

We can also write:

$$\frac{\left\|\underset{\sim}{K}^{\mathsf{T}}\vec{n}_{IJ} \wedge \overrightarrow{x_{\hat{L}}x_{\hat{L},i(IJ)}}\right\|}{\left\|\underset{\sim}{K}^{\mathsf{T}}\vec{n}_{IJ}\right\|\left\|\overrightarrow{x_{\hat{L}}x_{\hat{L},i(IJ)}}\right\|} = \sin\left(\theta^1_{\hat{L},IJ}\right) \tag{14}$$

After some algebraic manipulation of Equations (13) and (14), we get:

$$\alpha_{\hat{L},j(IJ)} = \frac{\left\|\underset{\sim}{K}^{\mathsf{T}}\vec{n}_{IJ}\right\|\sin\left(\theta^1_{\hat{L},IJ}\right)}{\left\|\overrightarrow{x_{\hat{L}}x_{\hat{L},j(IJ)}}\right\|\sin\left(\theta^1_{\hat{L},IJ} + \theta^2_{\hat{L},IJ}\right)} \tag{15}$$

where $\left|\alpha_{\hat{L},j(IJ)}\right| = \alpha_{\hat{L},j(IJ)} \geq 0$, because the angles satisfy the following conditions $0 < \theta^1_{\hat{L},IJ} \leq \pi$ and $\theta^1_{\hat{L},IJ} + \theta^2_{\hat{L},IJ} \leq \pi$. Using a similar argument to calculate the parameter $\alpha_{\hat{L},i(IJ)}$:

$$\alpha_{\hat{L},i(IJ)} = \frac{\left\|\underset{\sim}{K}^{\mathsf{T}}_{\hat{L}}\vec{n}_{IJ}\right\|\sin(\theta^2_{\hat{L},IJ})}{\left\|\overrightarrow{x_{\hat{L}}x_{\hat{L},i(IJ)}}\right\|\sin(\theta^1_{\hat{L},IJ} + \theta^2_{\hat{L},IJ})} \tag{16}$$

where $\left|\alpha_{\hat{L},i(IJ)}\right| = \alpha_{\hat{L},i(IJ)} \geq 0$, because the angles satisfy the following conditions $0 < \theta^2_{\hat{L},IJ} \leq \pi$ and $\theta^1_{\hat{L},IJ} + \theta^2_{\hat{L},IJ} \leq \pi$.

Summing up, in the previous equations, the coefficients $\alpha_{\hat{L},i(IJ)}$, $\alpha_{\hat{L},j(IJ)}$ exist and are non-negative when the angles formed by segments $\overrightarrow{x_{\hat{L}}x_{\hat{L},i(IJ)}}$ (resp. $\overrightarrow{x_{\hat{L}}x_{\hat{L},j(IJ)}}$) and the co-normal $\underset{\sim}{K}^{\mathsf{T}}_{\hat{L}}\vec{n}_{IJ}$, satisfies the following conditions: $0 < \theta^1_{\hat{L},IJ}$, $\theta^2_{\hat{L},IJ} \leq \pi$ and $\theta^1_{\hat{L},IJ} + \theta^2_{\hat{L},IJ} \leq \pi$ (see figure 2a), therefore $\alpha_{\hat{L},i(IJ)} + \alpha_{\hat{L},j(IJ)} \geq 0$. It is worth mentioning, that our scheme is not monotone, because non-negative coefficients is a necessary but not sufficient condition to assure the monotone or extremum-preserving properties of this type of method (Le Potier, 2005; Lipnikov et al., 2007; Yuan and Sheng, 2008; Gao and Wu, 2013).

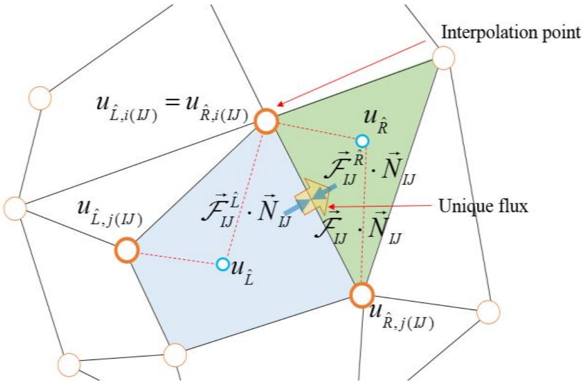

Figure 2. Represent the one-sided flux's, the unique flux and auxiliary variables.

Inserting Eq. (10) into Eq. (9), we obtain the following equation

$$\int_{IJ} \vec{\mathcal{F}} \cdot \vec{n}_{IJ} \mathrm{ds} = -\int_{IJ} \left(\alpha_{\hat{L},i(IJ)} \nabla u \cdot \overrightarrow{x_{\hat{L}} x_{\hat{L},i(IJ)}} + \alpha_{\hat{L},j(IJ)} \nabla u \cdot \overrightarrow{x_{\hat{L}} x_{\hat{L},j(IJ)}} \right) \mathrm{ds} \tag{17}$$

To construct the one-sided flux, we use a local finite difference method to approximate the partial derivatives ∇u along directions $\overrightarrow{x_{\hat{L}} x_{\hat{L},i(IJ)}}$ and $\overrightarrow{x_{\hat{L}} x_{\hat{L},j(IJ)}}$ (Yuan and Sheng, 2008), as shown in the following equation:

$$\vec{\mathcal{F}}_{IJ}^{\hat{L}} \cdot \vec{N}_{IJ} = -\left\| \overrightarrow{IJ} \right\| \left(\alpha_{\hat{L},i(IJ)} \left(u_{\hat{L},i(IJ)} - u_{\hat{L}} \right) + \alpha_{\hat{L},j(IJ)} \left(u_{\hat{L},j(IJ)} - u_{\hat{L}} \right) \right) \tag{18}$$

where the one-sided flux $\int_{JI} \vec{\mathcal{F}} \cdot \vec{n}_{JI} \mathrm{ds} = \vec{\mathcal{F}}_{IJ}^{\hat{L}} \cdot \vec{N}_{JI}$ is represented in figure 2.

In compact form, we can write:

$$\vec{\mathcal{F}}_{IJ}^{\hat{L}} \cdot \vec{N}_{IJ} = \left\| \overrightarrow{IJ} \right\| \left(\psi_{\hat{L},IJ} u_{\hat{L}} - \sum_{\gamma=i,j} \alpha_{\hat{L},\gamma(IJ)} u_{\hat{L},\gamma(IJ)} \right) \quad \text{and} \quad \psi_{\hat{L},IJ} = \alpha_{\hat{L},i(IJ)} + \alpha_{\hat{L},j(IJ)} \tag{19}$$

satisfying $\psi_{\hat{L},IJ} > 0$.

Similarly, we calculate the one-sided flux with respect to control volume $\hat{R}$ (see figure 2), as:

$$\vec{\mathcal{F}}_{IJ}^{\hat{R}} \cdot \vec{N}_{JI} = \left\| \overrightarrow{IJ} \right\| \left(\psi_{\hat{R},IJ} u_{\hat{R}} - \sum_{\gamma=i,j} \alpha_{\hat{R},\gamma(IJ)} u_{\hat{R},\gamma(IJ)} \right) \quad \text{and} \quad \psi_{\hat{R},IJ} = \alpha_{\hat{R},i(IJ)} + \alpha_{\hat{R},j(IJ)} \tag{20}$$

satisfying $\psi_{\hat{R},IJ} > 0$.

In equations (19) and (20) the auxiliary variables are denoted by $u_{\hat{R},\gamma(IJ)}$, $u_{\hat{L},\gamma(IJ)}$ and represented in figure 2.

3.1.1 Construction of the unique control surface flux

In order to construct a conservative scheme, we use the one-side fluxes defined in equations (19) and (20) to define the unique flux on the face (*IJ*), therefore:

$$\vec{\mathcal{F}}_{IJ} \cdot \vec{N}_{IJ} = w_{\hat{R},IJ} \vec{\mathcal{F}}_{IJ}^{\hat{L}} \cdot \vec{N}_{IJ} - w_{\hat{L},IJ} \vec{\mathcal{F}}_{IJ}^{\hat{R}} \cdot \vec{N}_{JI} \tag{21}$$

The weights $w_{\hat{L},IJ}$ and $w_{\hat{R},IJ}$ are defined as:

$$w_{\hat{R},IJ} = \frac{\psi_{\hat{R},IJ}}{\psi_{\hat{L},IJ} + \psi_{\hat{R},IJ}} \quad \text{and} \quad w_{\hat{L},IJ} = \frac{\psi_{\hat{L},IJ}}{\psi_{\hat{L},IJ} + \psi_{\hat{R},IJ}} \tag{22}$$

The fluxes given in the equations (19) and (20) are introduced into equation (21), and, after some algebraic manipulation, we have the following unique flux:

$$\vec{\mathcal{F}}_{IJ} \cdot \vec{N}_{IJ} = \tau_{IJ} \left(u_{\hat{L}} - u_{\hat{R}} - \sum_{\gamma=i,j} \kappa_{\hat{L},\gamma(IJ)} u_{\hat{L},\gamma(IJ)} - \kappa_{\hat{R},\gamma(IJ)} u_{\hat{R},\gamma(IJ)} \right) \tag{23}$$

where $\tau_{IJ} = \left\| \overrightarrow{IJ} \right\| \dfrac{\psi_{\hat{R},IJ} \psi_{\hat{L},IJ}}{\psi_{\hat{R},IJ} + \psi_{\hat{L},IJ}}$, $\kappa_{\hat{R},\gamma(IJ)} = \dfrac{\alpha_{\hat{R},\gamma(IJ)}}{\psi_{\hat{R},IJ}}$ and $\kappa_{\hat{L},\gamma(IJ)} = \dfrac{\alpha_{\hat{L},\gamma(IJ)}}{\psi_{\hat{L},IJ}}$.

Remark 1. In *K*-orthogonal grids, the discrete flux given in equation (23) will result in a TPFA scheme.

3.1.2 Treatment of boundary fluxes

For control surfaces (IJ) over boundaries $\Gamma_D \subset \mathcal{E}_{\hat{L}} \cap \mathcal{E}^{ext}$ with prescribed scalar variable (Dirichlet boundary conditions) and considering equation (15), we have:

$$\vec{\mathcal{F}}_{IJ} \cdot \vec{N}_{IJ} = \vec{\mathcal{F}}_{IJ}^{\hat{L}} \cdot \vec{N}_{IJ} = \tau_{IJ} u_{\hat{L}} - \left\| \overrightarrow{IJ} \right\| \sum_{\gamma=i,j} \alpha_{\hat{L},\gamma(IJ)} u_{\hat{L},\gamma(IJ)} \tag{24}$$

where $\tau_{IJ} = \left\| \overrightarrow{IJ} \right\| \left(\alpha_{\hat{L},i(IJ)} + \alpha_{\hat{L},j(IJ)} \right)$ is defined in equation (19).

For control surfaces (*IJ*) over boundaries $\Gamma_N \subset \mathcal{E}_{\hat{L}} \cap \mathcal{E}^{ext}$ with imposed fluxes (Neumann boundary conditions) and again, considering equation (15), we can write:

Proceedings of the XXXVIII Iberian Latin-American Congress on Computational Methods in Engineering
P.O. Faria, R.H. Lopez, L.F.F. Miguel, W.J.S. Gomes, M. Noronha (Editores), ABMEC, Florianópolis, SC, Brazil, November 5-8, 2017.

$$\vec{\mathcal{F}}_{IJ} \cdot \vec{N}_{IJ} = -\bar{g}_{N,IJ} \left\| \overrightarrow{IJ} \right\| \tag{25}$$

in equation (25) the normal flux on Γ_N is given by the mean value $\bar{g}_{N,IJ}$.

Remark 2. In our scheme, the choice of the interpolation points depends on the co-normal direction ($\underset{\sim}{K}_{\hat{L}}^{\mathsf{T}} \vec{n}_{IJ}$), see figure. 1 and 2. Therefore, whenever handling boundary conditions, if the co-normal intersects the correspondent boundary face ($\underset{\sim}{K}_{\hat{L}}^{\mathsf{T}} \vec{n}_{IJ} \cap \overrightarrow{IJ}$, $IJ \in \mathcal{E}_{\hat{L}} \cap \mathcal{E}^{ext}$) as shown in Fig. 3a, the pressure in the vertex of the face are provided when $IJ \in \Gamma_D$, or when $IJ \in \Gamma_N$ the pressures are interpolated (Gao and Wu, 2011). In severely anisotropic medium the co-normal can intersect an inner face ($\underset{\sim}{K}_{\hat{L}}^{\mathsf{T}} \vec{n}_{IJ} \cap \overrightarrow{IJ}$, $IJ \in \mathcal{E}_{\hat{L}} \cap \mathcal{E}^{\text{int}}$), see Fig. 3b for which only one vertex of the control surface belongs to the boundary.

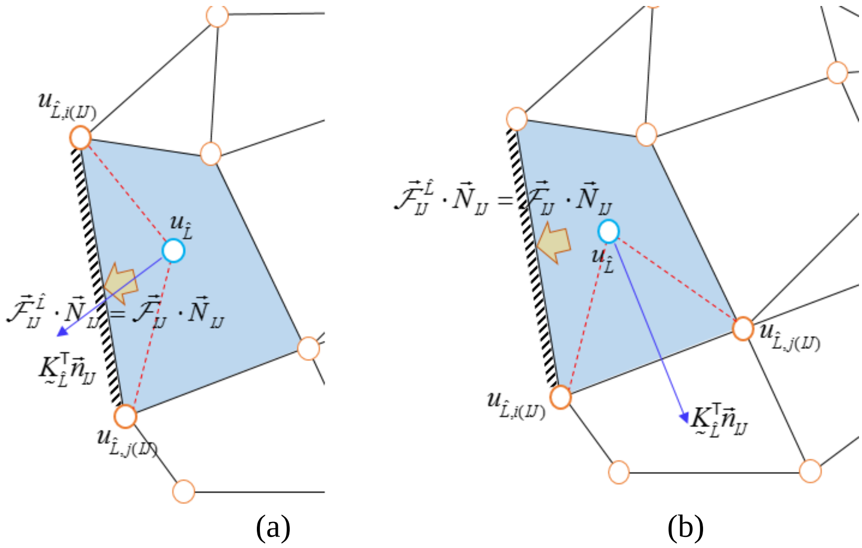

Figure 3. Schematic showing different boundary conditions.

3.1.3 Approximation of vertex-unknowns.

As previously mentioned, the scalar unknowns on mesh vertices can be written as linear weighted combinations of the neighboring cell-centered unknowns, so that the MPFA-HD scheme becomes a fully cell-centered finite volume formulation. In the present work, we used the explicit weight proposed in (Gao and Wu, 2011) and used in (Queiroz et al., 2014, Contreras et al., 2016). This weight is called “explicit” to indicate that the it is computed with no need to solve a set of local system of equations, as in others classic MPFA methods (Aavatsmark 1998, 2002, Edwards and Rogers 1998). Other authors have proposed various ways to calculate the interpolation weights, but, as pointed out by (Gao and Wu 2011), in general, these interpolations are not very robust in treating anisotropic and heterogeneous (possibly discontinuous) media. However, adopting the Linearity-Preserving Explicit Weighted (LPEW) interpolation, the

Proceedings of the XXXVIII Iberian Latin-American Congress on Computational Methods in Engineering
P.O. Faria, R.H. Lopez, L.F.F. Miguel, W.J.S. Gomes, M. Noronha (Editores), ABMEC, Florianópolis, SC, Brazil, November 5-8, 2017.

explicit weight in Eq. (26) is derived using the continuity equation throughout the auxiliary volumes or “interaction regions” built around each mesh vertex, by connecting the midpoints of adjacent mesh edges.

In this case, a general vertex (I) unknown can be expressed as:

$$u_I = \sum_{\hat{i}=1}^{ncv} w_{\hat{i}} u_{\hat{i}} \tag{26}$$

where $w_{\hat{i}}$ is the weight assigned to each control volume $\hat{i}$, more details in (Gao and Wu, 2011; Queiroz et al, 2014; Contreras et al, 2016).

4 NUMERICAL EXPERIMENTS

In this section, we present numerical result in order to show to efficiency, robust and accuracy of our scheme. Firstly, in order to show the accuracy and robustness of the proposed scheme, we briefly define the discrete L_2-norm to evaluate approximation errors. For instance, for the solution u, we use the following L_2-norm:

$$\varepsilon_u = \left(\sum_{\hat{L}\in\mathcal{M}} \left(u(\vec{x}_{\hat{L}}) - u_{\hat{L}} \right)^2 V_{\hat{L}} \Big/ \sum_{\hat{L}\in\mathcal{M}} V_{\hat{L}} \right)^{\frac{1}{2}} \tag{27}$$

and for the flux we use the following L_2-norm:

$$\varepsilon_{\mathcal{F}} = \left(\sum_{IJ\in\mathcal{E}} \left(\vec{\mathcal{F}}_n(\vec{x}_{IJ}) - \vec{\mathcal{F}}_{IJ} \right)^2 A_{IJ} \Big/ \sum_{IJ\in\mathcal{E}} A_{IJ} \right)^{\frac{1}{2}} \tag{28}$$

where the analytical solution and the analytical flux is denoted by $u(\vec{x})$ and $\vec{\mathcal{F}}_n(\vec{x}) = -\underset{\sim}{K}\nabla u(\vec{x})\cdot\vec{n}$, respectively. And A_{IJ} is a representative area associated with the edge IJ, more precisely, it is the sum of areas of the CVs sharing edge IJ. The numerical convergence rates $R_\gamma\left(\gamma = u, \mathcal{F}\right)$ are obtained by the following expression:

$$R_\gamma = \frac{\log\left(\varepsilon_\gamma(h_2)/\varepsilon_\gamma(h_1)\right)}{\log\left(h_2/h_1\right)} \tag{29}$$

where h_1, h_2 denote the sizes of two successive meshes and $\varepsilon_\gamma(h_1)$, $\varepsilon_\gamma(h_2)$ are the corresponding L_2-norms of the errors.

The maximum and minimum values of the pressure field are calculated using the following relation $u_{\max} = \max_{\hat{L}\in\mathcal{M}}\left\{u_{\hat{L}}\right\}$ and $u_{\min} = \min_{\hat{L}\in\mathcal{M}}\left\{u_{\hat{L}}\right\}$, respectively.

4.1 Linearity-preserving verification

This problem was adapted from Herbin and Hubert, (2008), with the aim of analyzing the linearity-preserving criterion on heterogeneous and anisotropic media. The domain is composed by follow domains:

$$\begin{aligned}
\Omega_1 &= \left\{\vec{x}\in\Omega : \psi_1(\vec{x}) < 0\right\} \\
\Omega_2 &= \left\{\vec{x}\in\Omega : \psi_1(\vec{x}) > 0 \text{ and } \psi_2(\vec{x}) < 0\right\} \\
\Omega_3 &= \left\{\vec{x}\in\Omega : \psi_2(\vec{x}) < 0\right\}
\end{aligned} \tag{30}$$

where $\psi_1(\vec{x}) = y - 0.2(x-0.5) - 0.475$, $\psi_2(\vec{x}) = \psi_1(\vec{x}) - 0.05$ and $\vec{x} = (x, y)\in\Omega$. In this problem, we consider a configuration in that to exact solution is given by $u(\vec{x}) = 2 - x - 0.2y$ in figure 4b we show the exact solution.

The outer contour coincides with the condition Dirichlet boundary and the diffusion tensor is presented in the following equation for each domain:

$$\underset{\sim}{K}(\vec{x}) = \mathcal{R}_\theta \begin{pmatrix} \alpha & 0 \\ 0 & \beta \end{pmatrix} \mathcal{R}_\theta^{-1} \tag{31}$$

where $\mathcal{R}_\theta$ is rotation matrix with angle $\theta = \arctan(0.2)$, $\alpha = 100$, $\beta = 10$ on Ω_2 and $\alpha = 1$, $\beta = 0.1$ on $\Omega_1 \cup \Omega_3$.

We discrete the domain using the oblique mesh (see figure 4a), and we obtained the following errors $\varepsilon_u = 1{,}0747\times10^{-15}$ and $\varepsilon_{\mathcal{F}} = 7.7901\times10^{-14}$ that are very close to the machine precision. Thus, we concluded that our MPFA-HD scheme is linearity-preserving.

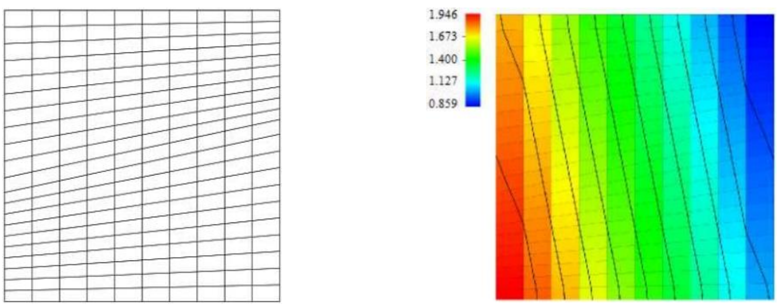

(a) (b)

Figure 4. (a) Oblique mesh, (b) exact solution.

4.2 Convergence test

This problem was adapted from Sheng and Yuan (2016), consists in a square domain of dimensions $[0,1]^2$. We consider permeability tensor that varies as a function of the position and is defined as:

$$\underset{\sim}{K}(\vec{x}) = \mathcal{R}_\theta \begin{pmatrix} k_1(\vec{x}) & 0 \\ 0 & k_2(\vec{x}) \end{pmatrix} \mathcal{R}_\theta^{-1} \quad \text{and} \quad \theta = 5\pi/12 \tag{32}$$

where $k_1(\vec{x}) = 1 + 2x^2 + y^2$, $k_2(\vec{x}) = 1 + x^2 + 2y^2$.

The analytical solution and the source term respectively are given by:

$$u(\vec{x}) = \sin(\pi x)\sin(\pi y) \tag{33}$$

and:

$$\begin{aligned} Q(\vec{x}) = {} & -4.9342(x^2 - y^2)cos(\pi x)cos(\pi y) + \pi^2(2 + 2.9998x^2 + 2.9998y^2)sin(\pi x)sin(\pi y) - \\ & \left(1.57061x + 6.70353y\right) sin(\pi x)cos(\pi y) - \left(6.70353x - 1.57061y\right) cos(\pi x)sin(\pi y) \end{aligned} \tag{34}$$

The Dirichlet boundary conditions are imposed by applying the analytical solution directly over the boundaries. In order to evaluate the robustness and accuracy of the proposed numerical scheme (MPFA-HD), we consider two meshes, as shown in figure 5. In addition, we compare our results with some classical MPFA schemes available in literature, namely MPFA-O (Aavatsmark, 2002) and MPFA-FPS (Edwards and Zheng, 2008). In tables 1, and 2, we present the errors and rates of convergence for a sequence of successively refined meshes

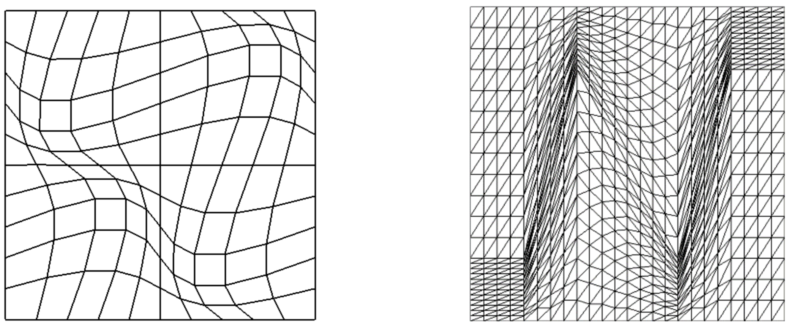

(a) (b)

Figure 5. Samples of the meshes used for simulations: (a) slightly distorted quadrilateral mesh with 100 cells, (b) Kershaw triangular mesh with 1152 cells.

Tables 1 give the errors and convergence rates of the MPFA-HD, O and FPS schemes on quadrilateral meshes (see figure 5a). From this table, we obtain too close second order accuracy

Proceedings of the XXXVIII Iberian Latin-American Congress on Computational Methods in Engineering
P.O. Faria, R.H. Lopez, L.F.F. Miguel, W.J.S. Gomes, M. Noronha (Editores), ABMEC, Florianópolis, SC, Brazil, November 5-8, 2017.

for the pressure field and greater that 1.5 accuracy for the flux, for the all methods (MPFA-HD, O and FPS).

Table 1. Convergence test: Comparison of errors and convergence rates for a sequence of successively refined meshes (slightly distorted).

Number of cells		100	400	1600	6400	25600
MPFA-HD	ε_u	0.0100	0.0025	6.3375x10^{-4}	1.5507x10^{-4}	3.7649x10^{-5}
	R_u	------	2.0000	1.9799	2.0309	2.0422
	$\varepsilon_{\mathcal{F}}$	0.0933	0.0262	0.0070	0.0019	5.2725x10^{-4}
	$R_{\mathcal{F}}$	------	1.8323	1.9041	1.8813	1.8494
MPFA-O	ε_u	0.0086	0.0021	5.2173x10^{-4}	1.2098x10^{-4}	2.3044x10^{-5}
	R_u	------	2.0339	2.0090	2.1085	2.3923
	$\varepsilon_{\mathcal{F}}$	0.0603	0.0153	0.0038	9.4431x10^{-4}	2.3475x10^{-4}
	$R_{\mathcal{F}}$	------	1.97862	2.0094	2.0086	2.0835
MPFA-FPS	ε_u	0.0099	0.0025	6.2945x10^{-4}	1.5295x10^{-4}	3.6087x10^{-5}
	R_u	------	1.9855	1.9896	2.0410	2.0835
	$\varepsilon_{\mathcal{F}}$	0.1037	0.0269	0.0069	0.0018	4.9496x10^{-4}
	$R_{\mathcal{F}}$	------	1.9467	1.9629	1.9386	1.8626

In table 2 our results are considered for Kershaw triangular mesh (see figure 5b), in this test we note that the accuracy of our scheme (MPFA-HD) is close to first order when the meshes are coarse. Similarly, the convergent rate for the pressure field is close to 2 and the convergent rate of the error for flux is close to 1.5 as the number of cells is increased. On other hand, we observe that for this type of problems the convergence of the MPFA-O and FPS schemes on mesh (5b) is lost completely.

4.3 Monotonicity test: oblique flow using boundary conditions with steep gradients

This problem was adapted from Gao and Wu, (2013). In this test, the main directions of the anisotropic permeability tensor are tilted with respect to the boundary conditions and the mesh. The computational domain is the unit square $[0,1]^2$, and the anisotropic permeability tensor is given by:

$$\underset{\sim}{K}(\vec{x}) = \mathcal{R}_\theta \begin{pmatrix} 1 & 0 \\ 0 & 10^{-4} \end{pmatrix} \mathcal{R}_\theta^{-1} \text{ and } \theta = 40^\circ \tag{35}$$

Table 2. Convergence test: Comparison of errors and convergence rates on Kershaw triangular mesh.

Number of cells		1152	4608	18432	73728	294912
MPFA-HD	ε_u	0.0358	0.0158	0.0052	0.0015	3.9340x10^{-4}
	R_u	-----	1.1800	1.6033	1.7935	1.9309
	$\varepsilon_{\mathcal{F}}$	0.5155	0.2284	0.0803	0.0257	0.0083
	$R_{\mathcal{F}}$	-----	1.1744	1.5081	1.6463	1.6306
MPFA-O	ε_u	0.0195	0.0062	0.0024	0.0010	6.8544x10^{-4}
	R_u	-----	1.6606	1.3673	1.2204	0.5
	$\varepsilon_{\mathcal{F}}$	0.2756	0.1100	0.0463	0.0693	0.100
	$R_{\mathcal{F}}$	-----	1.3250	1.2484	-0.5818	-0.5291
MPFA-FPS	ε_u	0.0159	0.0037	0.0011	3.6734x10^{-4}	1.4115x10^{-4}
	R_u	-----	2.1089	1.7766	1.5522	1.3798
	$\varepsilon_{\mathcal{F}}$	0.8862	0.3741	0.1512	0.0605	0.0239
	$R_{\mathcal{F}}$	-----	1.2440	1.3069	1.3214	1.3279

The source term $Q(\vec{x})=0$ for all $\vec{x}\in\Omega$ and the Dirichlet boundary conditions are considered, $u=g_D$ on $\partial\Omega$, with g_D a continuous and piecewise linear function defined by:

$$g_D=\begin{cases}1 \quad \text{on } (0,0.2)\times\{0\}\cup\{0\}\times(0,0.2)\\ 0 \quad \text{on } (0.8,1)\times\{1\}\cup\{1\}\times(0.8,1)\\ 0.5 \text{ on } (0.3,1)\times\{0\}\cup\{0\}\times(0.3,1)\\ 0.5 \text{ on } (0,0.7)\times\{1\}\cup\{1\}\times(0,0.7)\end{cases} \tag{36}$$

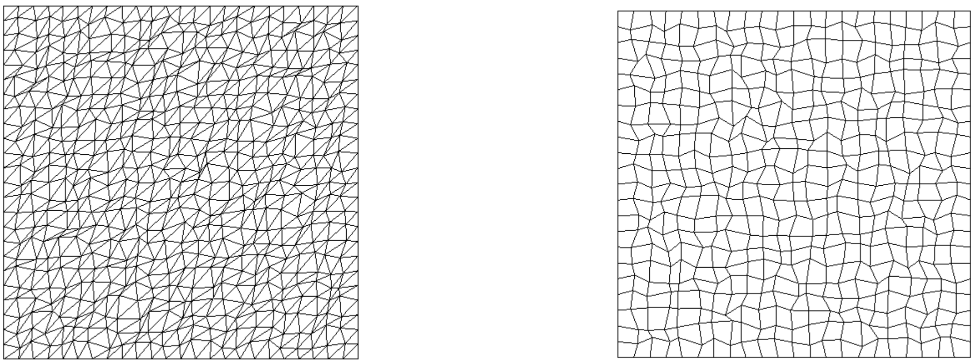

(a) (b)

Figure 6. (a) Random triangle and (b) random quadrilateral meshes both with $\tau=0.65$.

Proceedings of the XXXVIII Iberian Latin-American Congress on Computational Methods in Engineering
P.O. Faria, R.H. Lopez, L.F.F. Miguel, W.J.S. Gomes, M. Noronha (Editores), ABMEC, Florianópolis, SC, Brazil, November 5-8, 2017.

To solve this problem, we consider a randomly disturbed mesh, see figure 6. These meshes are constructed from the unitary square mesh by random distortion of its nodes denoted by x and y:

$$x = x + \tau\xi_x h,\; y = y + \tau\xi_y h \tag{37}$$

where ξ_x and ξ_y are random variables with values that belong to [-0.5, 0.5], h is the original spacing of the mesh and $\tau \in [0,1]$ is the degree of distortion.

The maximum principle states that the exact solution u should be bounded between 0 and 1 (Hopf's second lemma). The numerical pressure for the scheme MPFA-HD is depicted in figure 7a and 7d for random triangular and quadrilateral meshes, respectively. In both cases, the MPFA-HD scheme provides satisfactory results that satisfying the discrete extremum principle. In table 3, we can show that the MPFA-O scheme suffer spurious swings on random triangular mesh with 1152 control volumes (see figure 7b), violated the discrete maximum principle. These numerical oscillations do not disappear with refinement of the mesh (see table 3: random triangular and quadrilateral meshes with 18432 and 9216 control volumes, respectively). Similar behavior presents the MPFA-FPS scheme on random quadrilateral mesh (see table 3 and figure 7c and 7f). The satisfaction of the extremum principle or, at least, monotonicity is very important. For instance, a scheme that do not preserve monotonicity can lead to the violation of the entropy constraints of the second law of thermodynamics, which may lead to negative absolute pressures or non-physical oscillations in the pressure field (Sheng and Yuan 2016).

Table 3: Monotonicity test: Oblique flow using boundary conditions with steep gradients: maximum and minimum values of the pressure field.

Schemes	Random triangular mesh				Random quadrilateral mesh			
	1152		18432		576		9216	
	$u_{\max}$	$u_{\min}$	$u_{\max}$	$u_{\min}$	$u_{\max}$	$u_{\min}$	$u_{\max}$	$u_{\min}$
MPFA-HD	0.9919	0.0115	0.9983	0.0012	0.9894	0.0126	0.9972	0.0029
MPFA-O	1.1750	-0.1906	1.0480	-0.0656	0.9880	0.0119	1.0190	-0.0267
MPFA-FPS	1.1350	-0.0793	0.9984	0.0011	0.9829	0.0178	1.0900	-0.0799

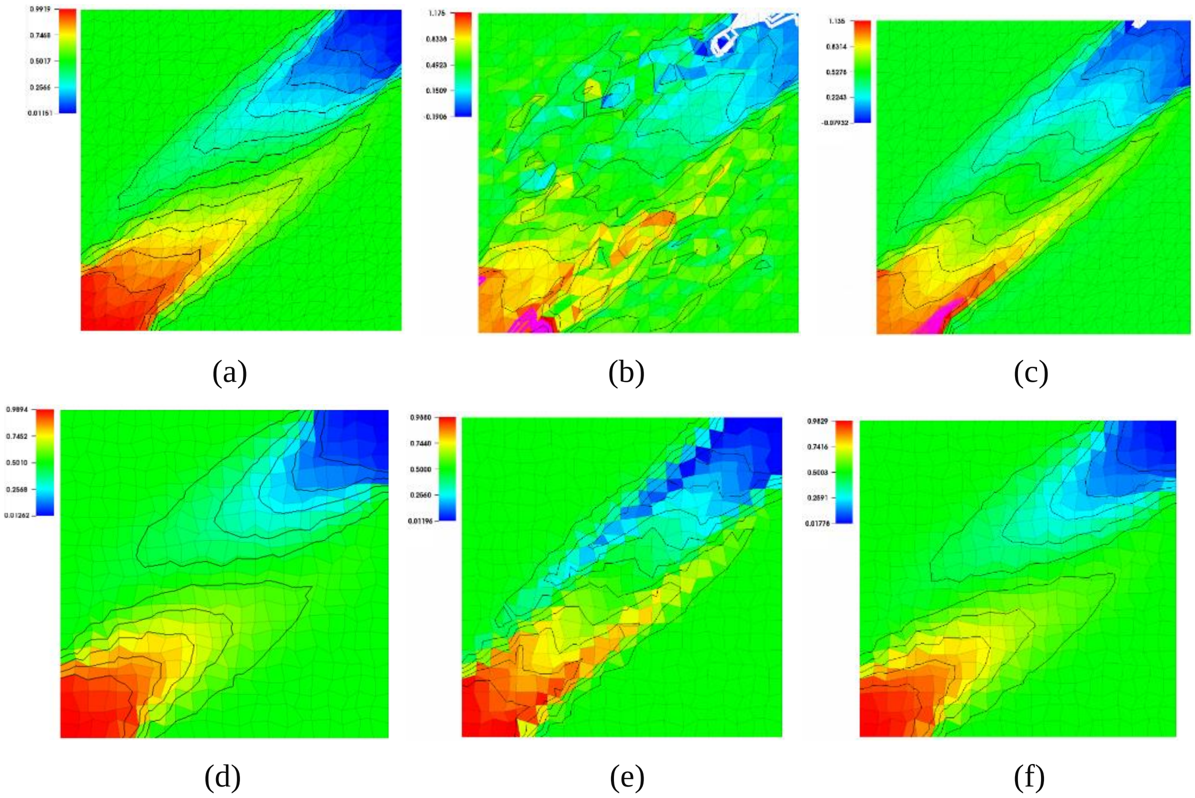

Figure 7. Pressure profiles obtained by: (a, d) MPFA-HD, (b, e) MPFA-O and (c, f) MPFA-FPS, where the pink color denotes values greater than 1 and the white color denotes negative values.

5 CONCLUSIONS

In this article, we have described a linear cell-centered and no orthodox MPFA-HD finite volume method to solve in one-phase problem in heterogeneous and anisotropic porous media using distorted meshes. The presented method is able to deal with any polygonal meshes by producing convergent solutions without the need for the solution of local systems which are common to other classical MPFA methods. This finite volume formulation is capable of handling highly heterogeneous, possibly discontinuous coefficients in an elegant and accurate manner. Some representative model examples were used in order to show the ability of the proposed method to deal with discontinuous permeability tensor that vary orders of magnitude throughout the domain. Several tests show the robustness of the proposed scheme (quadratic convergence rate for the approximate solution and higher than first-order accuracy for the flux), and the new proposed scheme seems to be more robust and accurate than both, the classical MPFA-O and the MPFA-FPS methods for 2-D diffusion problems.

ACKNOWLEDGEMENTS

The authors would like to thank the following Brazilian research agencies: Brazilian National Counsel of Technological and scientific Development (CNPq) and CENPES-PETROBRAS (SIGER-Petrobras Network on Simulation and Management of Petroleum Reservoirs).

REFERECES

Aavatsmark, I., et al., 1998. Discretization on unstructured grids for inhomogeneous, anisotropic media. Part II: Discussion and numerical results. *SIAM Journal on Scientific Computing* 19.5: 1717-1736.

Aavatsmark, I., 2002. An introduction to multipoint flux approximations for quadrilateral grids. *Computational Geosciences*, v. 6, n. 3, p. 405-432.

Aavatsmark, I., Eigestad, G. T., Mallison, B. T., & Nordbotten, J. M., 2008. A compact multipoint flux approximation method with improved robustness. *Numerical Methods for Partial Differential Equations*, *24*(5), 1329-1360.

Contreras, F. R. L., Lyra, P. R. M., Souza, M. R. A. & Carvalho, D. K. E., 2016. A cell-centered multipoint flux approximation method with a diamond stencil coupled with a higher order finite volume method for the simulation of oil–water displacements in heterogeneous and anisotropic petroleum reservoirs. *Computers & Fluids*, *127*, 1-16.

Chang, L., 2014. A reconstruction algorithm with flexible stencils for anisotropic diffusion equations on 2D skewed meshes. *Journal of Computational Physics*, v. 256, p. 484-500.

de Carvalho, D. K. E., Willmersdorf, R. B., & Lyra, P. R. M., 2007. A node-centred finite volume formulation for the solution of two-phase flows in non-homogeneous porous media. *International journal for numerical methods in fluids*, *53*(8), 1197-1219.

Droniou, J., 2014. Finite volume schemes for diffusion equations: introduction to and review of modern methods. *Mathematical Models and Methods in Applied Sciences* 24.08: 1575-1619.

Edwards, M. G., & Rogers, C. F., 1998. Finite volume discretization with imposed flux continuity for the general tensor pressure equation. *Computational Geosciences*, v. 2, n. 4, p. 259-290.

Eymard, R., Thierry G., & Raphaèle, H., 2000. *Finite volume methods*. Handbook of numerical analysis 7: 713-1018.

Gao, Z., & Wu, J., 2011. A linearity-preserving cell-centered scheme for the heterogeneous and anisotropic diffusion equations on general meshes. *International Journal for Numerical Methods in Fluids* 67.12: 2157-2183.

Gao, Z., & Wu, J., 2013. A small stencil and extremum-preserving scheme for anisotropic diffusion problems on arbitrary 2D and 3D meshes. *Journal of Computational Physics*, v. 250, p. 308-331.

Herbin, R., & Hubert, F., 2008. Benchmark on discretization schemes for anisotropic diffusion problems on general grids. In: Finite volumes for complex applications V. Wiley. p. 659--692.

Le Potier, C., 2005. Finite volume scheme for highly anisotropic diffusion operators on unstructured meshes. *Comptes Rendus Mathematique*, 921-926.

Nordbotten, J. M., & Aavatsmark, I., 2005. Monotonicity conditions for control volume methods on uniform parallelogram grids in homogeneous media. *Computational Geosciences* 9.1: 61-72.

Nordbotten, J. M., Aavatsmark, I., & Eigestad, G. T., 2007 Monotonicity of control volume methods. *Numerische Mathematik* 106.2: 255-288.

Queiroz, L. E. S., Souza, M. R. A., Contreras, F. R. L., Lyra, P. R. M., & Carvalho, D. K. E., 2014. On the accuracy of a nonlinear finite volume method for the solution of diffusion problems using different interpolations strategies. *International Journal for Numerical Methods in Fluids*, *74*(4), 270-291.

Sheng, Z., & Yuan, G., 2011. The finite volume scheme preserving extremum principle for diffusion equations on polygonal meshes. *Journal of Computational Physics* 230.7: 2588-2604.

Sheng, Z., & Yuan, G., 2016. A new nonlinear finite volume scheme preserving positivity for diffusion equations. *Journal of Computational Physics*, v. 315, p. 182-193.

Wu, J., & Gao, Z., 2014. Interpolation-based second-order monotone finite volume schemes for anisotropic diffusion equations on general grids. *Journal of Computational Physics*, v. 275, p. 569-588.

Yuan, G., & Sheng, Z., 2008. Monotone finite volume schemes for diffusion equations on polygonal meshes. *Journal of Computational Physics*, 227:6288–6312.

Yuan, G., & Sheng, Z., 2008. Calculating the vertex unknowns of nine point scheme on quadrilateral meshes for diffusion equation. *Science in China Series A: Mathematics* 51.8: 1522-1536.